Experimental Investigation of the Effect of Particle Cohesion on the Flow Dynamics in a Spheronizer

J. Bouffard, A. Cabana, J. Chaouki, and F. Bertrand
Dept. of Chemical Engineering, École Polytechnique de Montréal, QC H3C 3A7, Canada

DOI 10.1002/aic.13955
Published online November 26, 2012 in Wiley Online Library (wileyonlinelibrary.com).

The effect of particle cohesion on the flow dynamics inside a spheronizer is investigated by means of a recent technique developed in our group, which relies on the polymer coating of the particles. It is shown that the interparticle forces can be controlled with the temperature and the coating thickness, as is also confirmed by measurements of the dynamic density of the particle bed. Four different flow states were observed as the level of interparticle forces was increased. The results are reported in a flow map that compares the forces that come into play in the spheronizer with other interparticle forces encountered during wet granulation processes. By isolating the impact of the cohesive forces on granulation, these results show the potential of the polymer coating technique to study the effect of particle cohesion on the flow patterns in such processes. © 2012 American Institute of Chemical Engineers *AIChE J,* 59: 1491–1501, 2013
Keywords: granular flow, cohesion, spheronizer, temperature control, surface modification, agglomerates

Introduction

The cohesive particle flow behavior encountered in different applications, such as granulation or particle mixing, has an impact on the performance of these processes.[1–3] In the case of dry powder mixing, in tumblers for example, the interparticle forces change with respect to the particle-size distribution (PSD) or from the build-up of electrical charges if the blender is not grounded appropriately.[4] The particle properties, such as size, do not change significantly during the mixing process and the interparticle forces remain almost constant. On the other hand, other processes (e.g., granulation or milling) change the PSD, which modifies the interparticle forces. In the case of granulation, the change of cohesion is also affected by an increase in the binding agent concentration.[5] The granulation processes were considered for a long time as perfectly mixed systems and were modeled accordingly before it became obvious that the particle flow had an impact on the product obtained.[6–9] The particle flow affects the velocity gradient as well as the collisional and the residence times of the particles, which vary between the different areas of a granulator. Also, the way the shear stress propagates throughout the particle bed and the presence of dead zones are examples of the many factors affecting how the PSD evolves with respect to time in such processes.

In addition, segregation is subject to occur when the PSD is not monodispersed. This has been observed and characterized for various equipments used for granulation, such as rotary drums,[10] rotating pans,[11] vertical high-shear mixers,[12] rotor-processors, and fluidized beds.[13] Size segregation will cause an alteration of the frequency of collisions between granules of different sizes and their associated velocities. It can also cause a nonhomogeneous distribution of the binder agent, which can favor the larger particles that pass more frequently in the spraying area than their smaller counterparts. The ability to predict the intensity of the different granulation mechanisms (e.g., nucleation, coalescence, or breakage) then depends on the knowledge of the flow patterns of the segregated particles and their corresponding velocity scales within the different flowing zone of the equipment.

The characterization of the particle flow patterns within granulators is not an easy task because the flow field continuously changes over time from the modification of the particle properties. The time scale of granulation runs is typically less than half an hour for laboratory granulators (e.g., high-shear mixers or fluid-bed granulators). Due to such a short-time scale, it is challenging to accumulate enough data that are representative of the particle flow at specific times during the process. This time-scale problem could be circumvented if one had a means to adjust the interparticle forces independently of the particle properties. It would then be possible to mimic the flow behavior observed in granulation equipments at specific operation times.

In a previous paper, we proposed a new approach to introduce cohesive forces between particles without affecting their PSD while being processed in powder equipments.[14] This approach consists of coating on the particles a uniform layer of an amorphous copolymer [poly ethyl acrylate (PEA)/poly methyl methacrylate (PMMA)] characterized by a low-glass transition temperature. It was shown that, due to changes in the polymer properties, it is possible to increase the cohesive forces between particles by increasing the temperature. The level of intensity of these forces depends on the molecular interdiffusion rate of the polymer chains and the particle contact time. The time required to reach the

Correspondence concerning this article should be addressed to J. Chaouki at jamal.chaouki@polymtl.ca.

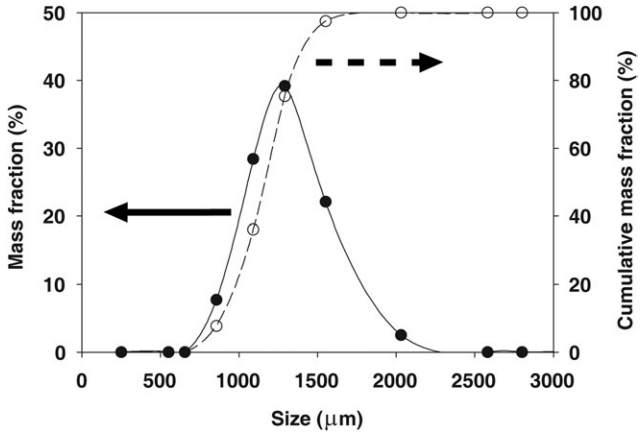

Figure 1. Particle-size distribution.[14]

maximum adhesive force can be approximated by the reptation time τ_D,[15] which can be estimated from the William–Landel–Ferry empirical model

$$\log\left(\frac{\tau_D}{\tau_R}\right) = \frac{-c_1(T - T_R)}{c_2 + (T - T_R)}, \tag{1}$$

where τ_R is the reference reptation time known at temperature T_R, T is the temperature, and c_1 and c_2 are regression constants that depend on the polymer species. When the polymer chains diffuse through the interfaces, the resultant adhesion force increases, which means that it depends on the time during which the particles are in contact. The estimation of the particle contact time t_c, is discussed in Ref. 14 and can be evaluated by the following relationship[16]

$$t_c = 2.94\left(\frac{5\sqrt{2}\pi\rho}{4}\frac{1-\upsilon^2}{E}\right)^{2/5}\frac{a}{{v_n}^{1/5}}, \tag{2}$$

where ρ is the particle density, υ is the Poisson ratio, E is the Young's modulus, a is the particle radius, and v_n is the normal collision velocity, which is estimated by the product of the particle size and the shear rate ($v_n = a\dot{\gamma}$).[17] Once it has been estimated, it can be used to calculate an effective adhesion energy W, from the maximum value of this adhesion energy W_m[18]

$$W = W_m[1 - \exp(-at_c^b)], \tag{3}$$

where the regression constants a and b vary with the polymer properties. This adhesive energy can then be used to evaluate the interparticle force F_{adh}, on the basis of the Johnson-Kendall-Roberts (JKR) theory for spherical polymer-coated particles.[14,19–21] Note that Eqs. 1–3 could be used for other thermoplastic materials by adjusting adequately the parameters and regression constants appearing in these equations.

Dimensional analysis can be used to describe the bonding regime that characterizes the separation of coated particles. The first dimensionless number is the Bond number (Bo) which is the ratio between the adhesive force binding the particles and the particle weight. A modified Bond number is used here to take into account not only the impact of the weight of the particle, but also the shear rate in the equipment

$$\text{Bo} = \frac{F_{\text{adh}}}{\sqrt{(m_p g)^2 + (2m_p R\dot{\gamma}^2)^2}}, \tag{4}$$

where R and m_p are the particle radius and mass and g is the gravitational constant. The second dimensionless number is the Deborah number (De)

$$\text{De} = \frac{V_d\tau_D}{h_0}, \tag{5}$$

where the ratio of the debonding velocity to the initial polymer layer thickness V_d/h_0, which corresponds to the average initial strain rate, can be approximated by the shear rate $\dot{\gamma}$. This dimensionless number is then the ratio of the reptation time to a characteristic process time ($1/\dot{\gamma}$).

The objective of this work was to apply the technique we introduced in Ref. 14, which is based on the polymer coating of particles and temperature control, to investigate the effect of particle cohesion on the flow dynamics inside a spheronizer. Note that while varying the temperature may also affect particle properties such as the friction factor (it is expected to increase with an increase of temperature) or the normal dissipation (it is expected to decrease with an increase of temperature), it is assumed that the impact on particle cohesion is more significant. The flow patterns in this device are representative of those found in rotor-based granulator equipments (e.g., the flat standard rotor used with the rotor granulators from Glatt and the conical rotor used with the Granurex® from Freund Vector). The use of a spheronizer simplifies the investigation of the flow patterns as the particles are pushed toward the wall of the equipment due to the centrifugal force. The toroid shape thus created is assessed by measuring the surface profile with a laser sheet profiler.[14] The effect of particle cohesion is investigated by measuring the changes of the surface position and analyzing the surface fluctuations caused by the presence of agglomerates when the particle adhesion is strong enough. The impacts of the process temperature and the polymer coating thickness on the particle cohesion are discussed and categorized as a function of the different flow behaviors observed. The impact of cohesion on the dynamic density of the particle bed is examined as it is related to the flowability of the particles within the equipment.[3,22] Finally, the results obtained in this work are discussed with regard to the flow dynamics in granulation equipments. To our knowledge, this is the first time that such a thorough experimental investigation of the particle flow behavior in a spheronizer has been realized.

Methodology

The experimental work first required the production of particles made of pharmaceutical excipients (by means of a wet powder process). These particles were then coated with a polymer film using an atomization process to obtain a uniform coating layer on their surface. After these preparation steps, the particulate material was used inside the spheronizer and submitted to different temperatures that altered the polymer properties and the cohesive forces.

Production of coated particles

The particles, which contained microcrystalline cellulose (MCC) and lactose monohydrate, were first produced with an extrusion-spheronization process. They are spherical, have a density of 1.5×10^3 kg m^3, and are characterized by a narrow PSD with a mean size of 1.2 mm, as shown in Figure 1.

The next step consisted of coating a polymer layer onto the surface of these particles. To achieve this task, a

Table 1. Coating Suspension of Eudragit® NE30D

Materials	Mass (%)
Water	68.5
PEA/PMMA 2:1	30.0
Nonoxynol 100	1.5

spheronizer (Caleva 380) was modified to incorporate an air line located below the rotating disc. Different batches were coated with a polymer suspension (Eudragit®) whose composition is indicated in Table 1. The PEA/PMMA copolymer ($T_g \approx -6°C$) in a molar ratio of 2–1 induces the cohesive effect while nonoxynol, a plasticizer, brings flexibility to the polymer. Different masses of polymer suspension, defined as high (H), medium (M), and low (L), were added to the batches without modification in the proportions indicated in Table 2. The coating layer thicknesses indicated were estimated by assuming an equal distribution of the polymer on all the particles while taking into account the PSD of Figure 1. The operation protocols used to produce and then coat the particles with Eudragit® is described in detail in Ref. 14. Note that the bonding between the pharmaceutical excipients in the particles and the coating layer is stronger than the one that would be obtained with common glass beads.

Measurement of the bed surface profile and spheronizer operation parameters

The impact of cohesion forces on the particle flow behavior inside the modified spheronizer that was used to coat the particles was assessed by measuring the surface position of the toroid shape obtained with the help of a line scanner profiler. The ScanControl 2800 laser line triangulation (LLT) (Micro-Epsilon) projects a laser sheet onto the particulate shape to triangulate its position. Figure 2 shows a schematic that explains how profile measurements were acquired. The position of the laser head was adjusted to project the laser sheet perpendicularly to the toroid surface and the distance from the particulate bed was chosen so that the complete profile of the toroid can be scanned. The laser scanner system operates according to the principle of optical triangulation (light intersection method). Once the laser line is projected onto the surface, the reflected light is replicated on a complementary metal-oxide-semiconductor (CMOS) array by a high quality optical system and evaluated in two dimensions (2-D). This equipment was set to give the accurate position of 512 points per profile with a height resolution of 40 μm at a frame rate of one profile per second. On the basis of experimental observations and the discrete element simulation of particle flow in the spheronizer,[23] the time interval was chosen to ensure that the toroidal shape had the time to reorganize between two measurements and that each profile was different from the previous one.

For each batch investigated, 50 profiles of the toroid surface were acquired with the line scanner profiler. After the experiments, the profiles were analyzed simultaneously with

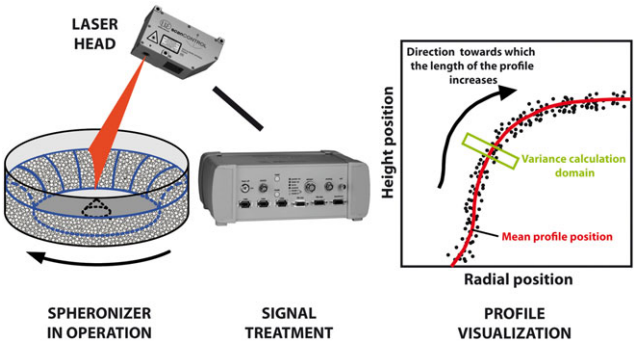

Figure 2. Surface measurement setup with the 2800-LLT ScanControl.

The box used to calculate the variance of the profile position is oriented so that the longer edge of the green rectangle is perpendicular to the mean profile. [Color figure can be viewed in the online issue, which is available at wileyonlinelibrary.com.]

an homemade Matlab® code that calculated the mean position of the toroid and its variance. Figure 2 shows the mean position as the line that crosses the cloud of points. The domain used to calculate the variance is represented by the green rectangular box. To investigate the periodic behavior of the toroid surface profile (see section Results and Discussion), the frame rate was increased to five profiles per second along with an acquisition duration higher than the characteristic period time related to the surface dynamics. The toroid surface position was acquired with the spheronizer operating parameters presented in Table 3. All the parameters were kept constant throughout the tests except for the temperature of the particulate bed, which was step incremented during each experiment, and the polymer coating thickness, which changed between the different batches. The range of temperatures selected was above the glass transition temperature of the polymer and was set to obtain a variation of the cohesive behavior of the flowing particles, which occurred above 25°C. The air flow rate coming from the bottom of the equipment was adjusted as indicated in Table 3; it was set to a low value to modify the temperature of the particles and to avoid infiltration of material below the rotating disc. To obtain a uniform temperature inside the spheronizer chamber, the bowl was closed with an acrylic cover on top of which an infrared captor was positioned toward the toroid surface. The measurement was taken when no temperature gradient was observed between the heated inlet air and the powder surface. An air flow rate between 12 and 15 cubic feet per minute (CFM) resulted in no significant changes on the particulate flow behavior when compared to an operation in absence of air flow.

Results and Discussion

The effects of the temperature and the coating thickness on the interparticle forces are discussed with the help of

Table 2. Final Particle Coating Characteristics

Materials	Batch H	Batch M	Batch L
Spherical particles (kg)	3.000	3.000	3.000
Eudragit coating (kg)	0.180	0.090	0.045
Percentage of coating (% wt)	7.3	3.0	1.5
Coating layer thickness (μm)	≈15	≈7	≈3.5

Table 3. Spheronizer Operating Parameters

Parameters	Values
Disc rotational rate (rpm)	230
Air flow rate (m^3/h)	20.4–25.5
Temperature range (°C)	25–45
Particle bed mass (kg)	3

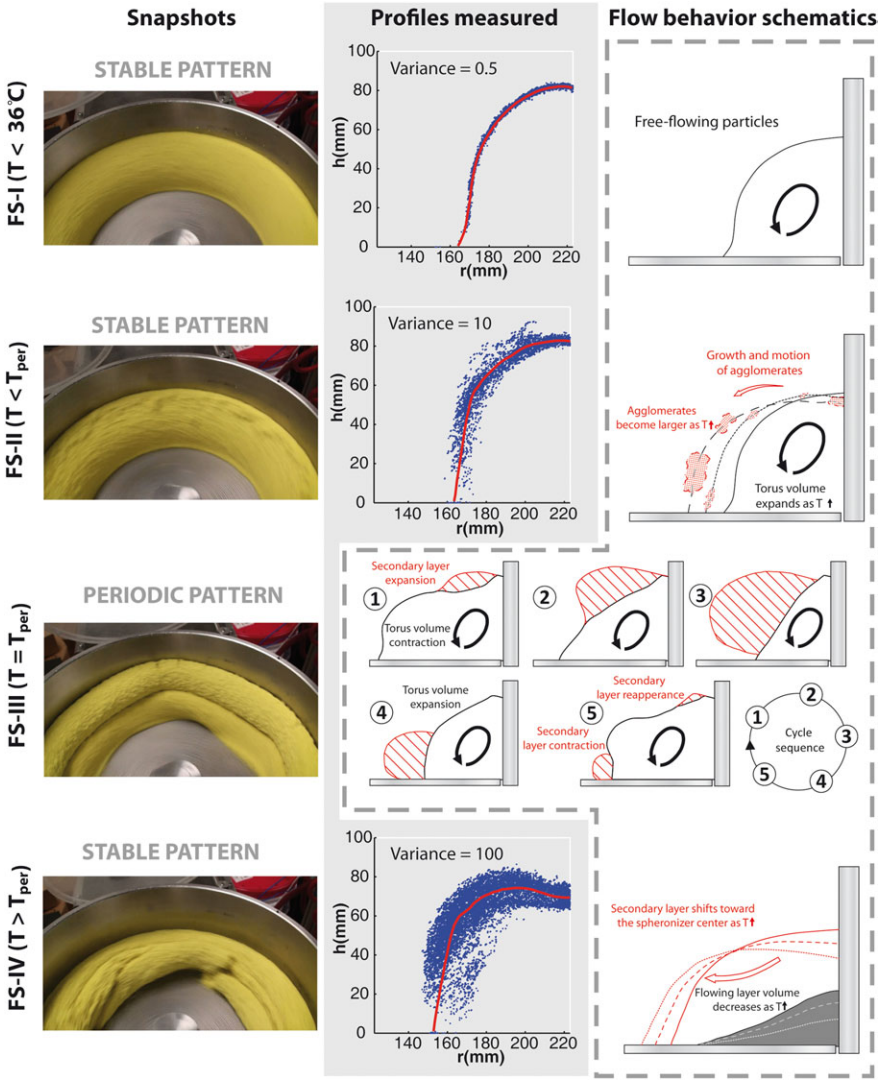

Figure 3. Flow states (FS) of the toroid as the temperature increases.

Snapshots taken with batch H are compared with the profiles obtained from the superposition of 50 measurements taken during each experiment. The variance indicated is related to the mean profile represented by the line passing trough the cloud of points. The schematics of the FS exaggerate the toroid profile variations to highlight how the temperature affects the particle bed shape and volume. Although for FS-I only a smooth flowing layer is indicated, the other states present either agglomerates (FS-II) indicated as shaded shapes, or a consolidated secondary layer (FS-III) represented as a hatched shape. The schematic for FS-IV represents the flowing and secondary layers using different colors. [Color figure can be viewed in the online issue, which is available at wileyonlinelibrary.com.]

measurements of the surface position and shape of the toroid as well as dynamic density data. Their effects on the particle bed flow behavior are next analyzed by comparing the results of batches **H**, **M**, and **L** (see Table 2). Finally, a so-called flow state map is introduced to provide more insight into results obtained and link them to the operating conditions of other granulation processes.

Influence of the temperature on the shape of the toroid

When the toroid is created with noncohesive material, the particles flow with a characteristic spiral motion in the azimuthal direction of the spheronizer.[14] Depending on the process temperature, the particulate bed can behave following four different states, as presented in Figure 3. Each state is accompanied with a representative snapshot taken during the experiments, a graph highlighting the mean, and the variance associated to the profiles measured by the laser sheet profiler, and a schematic of the cut-away view of the toroid changes as the temperature was incremented. No profile is presented for the third state because periodic patterns were observed in this case, as further explained below.

The first state (FS-I) was observed at ambient conditions and for temperatures below 36°C. FS-I corresponds to a toroid shape that remains stable with respect to time and is characterized by a free-flowing behavior of the particles. The toroid profile is not affected significantly by a change of temperature.

In the second state (FS-II), the toroid shape was also stable during the experiments. The difference from FS-I comes from the presence of isolated agglomerates at the toroid surface. As shown in Figure 3, the presence of these agglomerates has a significant impact on the variability of the toroid profiles measured. The schematic of FS-II also shows that the size of the agglomerates and the volume occupied by the

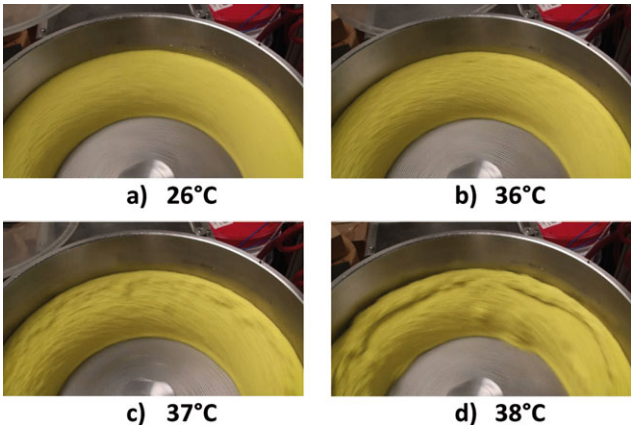

Figure 4. Snapshots of the toroid surface as the temperature was incremented in FS-II for batch H.

[Color figure can be viewed in the online issue, which is available at wileyonlinelibrary.com.]

toroid increase with the temperature. FS-II persisted until the temperature reached a threshold value (T_{per}) at which the isolated agglomerates gathered to form a secondary layer of particles.

The third state (FS-III) is a particular case as the toroid behavior is completely different from that of the other flowing states, which explains why it is treated differently in Figure 3. When the process temperature reaches the threshold value T_{per}, the particle flow changes significantly and the surface of the toroid becomes unstable with the occurrence of periodic fluctuations. FS-III was observed to persist over a narrow temperature range that depended strongly on the coating thickness.

The fourth state (FS-IV) presented an oscillatory but stable surface profile characterized by a solid mass motion of the toroid and occurred when the process temperature was above T_{per}.

The next three sections explain how the temperature affects the behavior of the particle flow for states FS-II–FS-IV. Because no significant changes were observed when the temperature was varied, FS-I is not further discussed.

Toroid flow state FS-II

As shown in Figure 4a, FS-I was observed when the temperature was near the ambient conditions and the particles were able to flow freely throughout the toroid domain. As the temperature was increased from 20 to 26°C, the surface of the toroid profile was not significantly affected. For batch **H**, FS-II appeared once the temperature reached 36°C (Figure 4b) with the presence of agglomerates at the surface of the bed, which increased in size as the upper temperature limit for FS-II (38°C) was approached (Figures 4c, d). The presence of these agglomerated particles caused variations on the position and the profile of the toroid measured with the laser scanner, which resulted in an increase of the variance around its mean position (Figure 3).

As can be seen in Figure 5a, the shape of the surface profile does not change significantly between 36 and 38°C. On the other hand, a comparison of the mean profile positions reveals small differences for this range of temperatures. In fact, a slight expansion of the volume of the toroid occurred when the temperature was increased. Figure 5b shows that the variance of the surface position is affected by the temperature (empty symbols), which can be explained by the increase in number and size of agglomerates at the surface of the toroid (see also Figure 3). At this level of temperature, it was observed that these agglomerates were short-lived as they got destroyed by the spheronizer disc when they flew toward it. Beyond 38°C, the flowing state FS-III appeared and the agglomerates were replaced by a secondary consolidated layer, as discussed in the next subsection. Such behavior is due to the effect of temperature on the magnitude of the interparticle cohesive forces resulting from the polymer coating at the surface of the particles.

For the temperature range covered in FS-II, the particles were constantly convected throughout the toroid. The appearance and the growth of the agglomerates with the temperature indicate a gradual increase of the cohesion forces between the particles. Three parameters contribute to the adhesive force between colliding particles: the contact area between the polymer layers, the particle contact time and the rate of interdiffusion of the polymer chains through the interface.[14] The contact area and the contact time are affected by

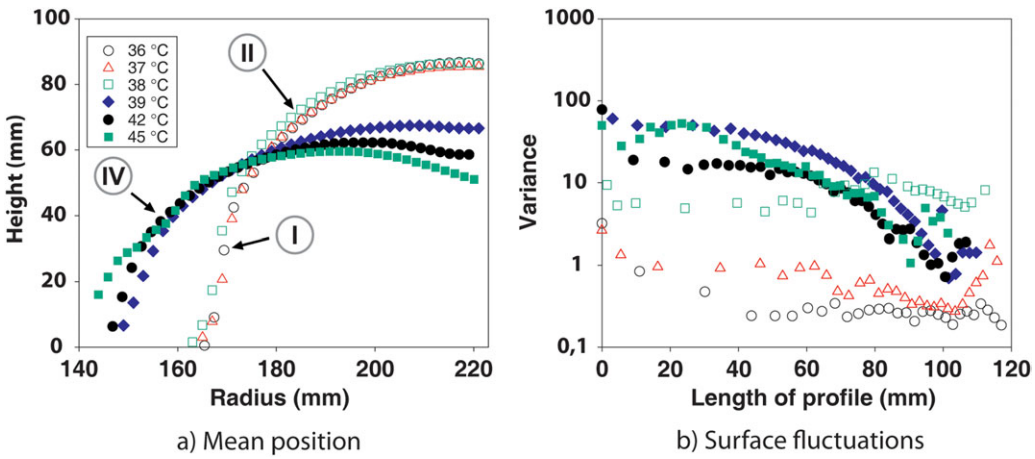

Figure 5. Surface position of the particle bed with respect to the temperature for batch H.

Empty symbols are related to FS-I and FS-II flow states while the solid symbols correspond to FS-IV. The graphs highlight the effect of temperature on (a) the mean position and (b) the variance of the surface profile. [Color figure can be viewed in the online issue, which is available at wileyonlinelibrary.com.]

the elastic modulus of the polymer. Its value is known to decrease with an increase of the temperature until it reaches a stable value that depends on the polymer properties.[24] For the PEA/PMMA copolymer, the elastic modulus stabilizes at 6×10^6 Pa around 35°C and remains around this value as the temperature is increased to 60°C.[25] The contact area and contact time are also affected by the pressure applied on the polymer layer during a collision. However, the pressure plays a lesser role in this work because the disk rotational rate remained the same for the experiments. For these reasons, the adhesive energy and the intensity of the interparticle forces are considered for FS-II to be mainly affected by the interdiffusion rate.

Toroid flow state FS-III

When the temperature reached a value higher than 38°C, a change of the flow structure became apparent as the agglomeration phenomena was replaced by the creation of a second flow layer. Beyond this temperature, the agglomerates disappeared at the surface of the toroid to be replaced by a consolidated layer of particles, on top of the original flowing layer, in the vicinity of the spheronizer wall, as shown in Figure 3. It resulted in two distinct zones with different flow behaviors. The bulk region, located at the bottom of the spheronizer, is characterized by a fast spiral-like motion of particles with no agglomerates. The second region, located on top of the first one, behaves differently, with particles that move as an apparent solid mass but at a slower pace. This zone has the properties of a dead zone, showing an absence of mixing and particles that remain trapped with no apparent interchange with the bulk region. In fact, FS-III was observed to be unstable because the two layers continually changed of shape and volume in a cyclic manner. Once created, the top layer increased in volume as the neighboring particles from the bottom layer were swallowed into it. The enlargement of the top layer continued until it reached the disc of the spheronizer and then collapsed, which caused the toroid to return to its initial state with one single bulk layer. After a short period of time, the top secondary layer reappeared and its volume expanded, initiating the beginning of a new cycle. Typical profiles observed during one cycle are presented later in this article for batch **M**. Note that measurements were difficult to obtain for batch **H** as the periodic behavior was somewhat blurred and appeared more sensitive to temperature. Once the temperature setpoint was reached, the behavior persisted for a short period of time before the flow state FS-III transited to FS-II or FS-IV depending on the temperature fluctuations in the spheronizer. Also note that FS-III was not observed for batch **L** (see Table 4).

The prolonged contact time of the particles in the secondary layer generates strong cohesion forces. This prevents a free flowing behavior and rather promotes the formation of a consolidated layer. The agglomerated particles can only be separated by the shear stress in the vicinity of the spheronizer disk. These cohesion forces surpass the shear forces at the surface of the toroid in FS-III. This explains the presence of the secondary layer and its cyclic behavior. The period of existence of this layer is related to a balance between the rate at which its volume expands and the time it takes to reach the high shear zone near the spheronizer disk where it is broken. The PEA/PMMA copolymer reptation time is not known; the measurement of this parameter could help clarify the evolution of the secondary layer by estimating the time-dependent magnitude of the cohesion forces prevailing in this layer, as discussed in section Introduction.

Table 4. Temperature Boundaries for the Four Different Flowing States with Respect to the Coating Thickness

Coating Thickness	FS-II (°C)	FS-III (°C)	FS-IV (°C)
H	36–38	38–39	39<
M	40–43	43–45	45<
L	44–50	50–?	–

Toroid flow state FS-IV

When the process temperature reached 39°C for batch **H**, the particulate bed moved as a solid mass with no apparent spiraling motion at the surface, which indicates that the cohesion forces have become larger than the inertial forces resulting from the shear provided by the rotating disc. As can be seen in Figure 5, the mean surface positions above 39°C are different from those at lower temperatures, with a lower height of the toroid near the wall of the spheronizer and an expansion of this toroid toward the center of this equipment as the temperature increases. The variances of the surface measurements along the length of the profiles are also different. The material located near the spheronizer disc is submitted to high stresses, which result in the rupture of the toroid surface in this vicinity and the formation of superimposed blocks of aggregated particles, as depicted in the corresponding schematic of Figure 3. The presence of these blocks and the associated fracture lines create a nonregular surface with peaks and valleys that explains the large values of the variance along the first half of the length of the surface profile in Figure 5. The snapshot for FS-IV in Figure 3 shows no blocks of particles in the vicinity of the spheronizer wall, hence the decrease of the variance in the second half of the surface profile length.

In FS-IV, the particles endures prolonged contact, which favors the increase of the adhesion forces. The absence of particle flow at the surface of the toroid means that, when this flow state is reached, the forces resulting from the shear rate induced by the spheronizer disc are inferior to the interparticle forces. The particle bed is then characterized by a quasistatic flow regime in which the particles flow as one single mass in the spheronizer. It is most probable that a thin layer of particles just above the spheronizer disc obeys a dense flow regime, although this phenomenon was not observed.

Influence of the coating thickness on the shape of the toroid

As explained earlier, the coating thickness was decreased from batches **H** to **L** (see Table 2). As the coating layer became thinner, a higher temperature was required to induce the different FS, as shown in Table 4. For batches **M** and **L**, that is for coating thicknesses of 7 and 3.5 μm, agglomerates were generated at process temperatures equal to 40 and 44°C, respectively. This tendency is confirmed by the results obtained for batch **H**, let alone for a coating thickness of 15 μm, where a temperature of 36°C was necessary to produce the first agglomerates. FS-II was observed between 40 and 43°C for batch **M** while it occurred between 44 and 50°C for batch **L**. Hence, decreasing the coating thickness of the polymer layer allowed the expansion of the range of temperatures at which FS-II was observed. Figures 6

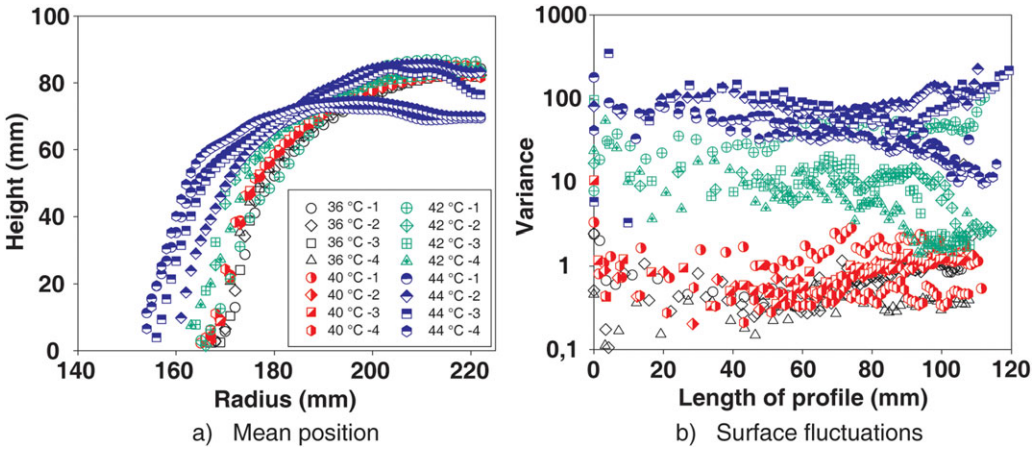

Figure 6. Surface position of the particle bed with respect to the temperature for batch M.

[Color figure can be viewed in the online issue, which is available at wileyonlinelibrary.com.]

(batch **M**) and 7 (batch **L**) show the mean positions of the toroid surface profiles and the associated variances for different temperatures and repetitions of the same experiment. All the profiles shown can be associated with FS-I or FS-II. It can be noticed that the decrease of the coating thickness led to a reduction in the variability of the results, especially as regards the variance measurements.

The numerous measurements made during these experiments indicate that the coating layer thickness has an impact on the existence of FS-III. For the batch **H**, FS-III occurred within a temperature range of 1°C, which prevented its stabilization. Because of that, FS-III was temporarily observed as FS-II transited to the FS-IV behavior. On the other hand, for batch **L**, the existence of the FS-III behavior was observed, but the characteristic period was difficult to estimate precisely as the layer at the top of the toroid was breaking at a varying rate. The cohesive forces, in this case, were outdone by the shear stresses present in the bulk layer, which prevented the creation of a coherent agglomerated structure at the top of the toroid. Contrary to the other two cases, state FS-III for batch **M** presented the periodic behavior depicted in Figure 8. The evolution of the top layer can be clearly observed in the insets associated with the profile curves. To ease the interpretation of the surface position profiles presented in this figure, schematics of the bulk (gray particles) and aggregated particle (red particles) layers have been added. When comparing the surface profiles measured at different times, one can see that the toroid returned to its initial shape between 14 and 16 s after the measurements started. In fact, this cycle repeated itself constantly for the temperature considered (≈44°C).

Influence of the toroid flow state on the dynamic density

The volume dilatation of a particle bed or the reduction of its bulk volume can be used to assess its flowability.[26,27] Noncohesive particles flow freely and give place to a slight expansion of the bed volume through collisional interference that increases the interparticle porosity. On the other hand, when flowing, cohesive particles generate soft agglomerates that roll over each other. As the intrinsic porosity of these agglomerates is larger than the one of a noncohesive particle bed, the volume expansion thus becomes more important as the interparticle forces increase. With the addition of a polymer coating on the particles, the volume of the particle bed changes depending on the interparticle forces induced, which increase with the temperature.[14] Indeed, it was in that previous paper that the dynamic density decreases with an increase of the temperature. Figure 9 shows the variation of the measured dynamic densities (mass of the particle bed divided by the volume of the toroid calculated from the

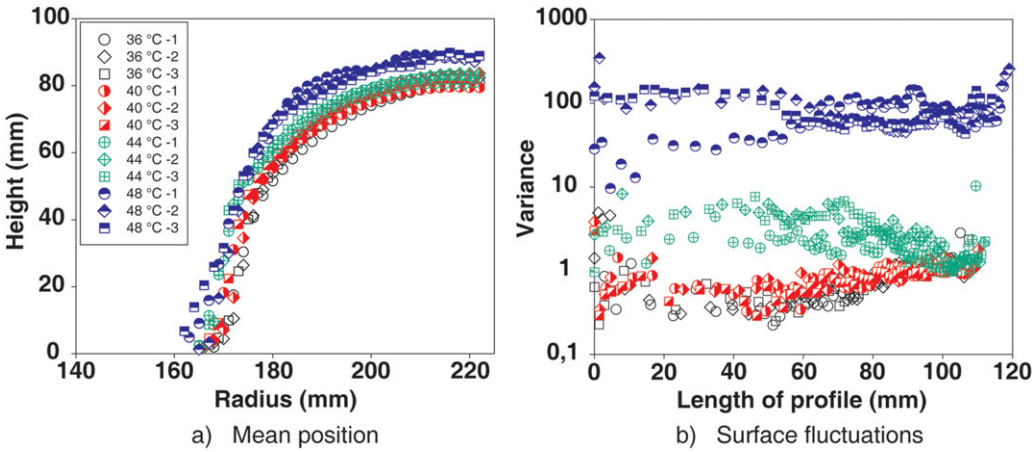

Figure 7. Surface position of the particle bed with respect to the temperature for batch L.

[Color figure can be viewed in the online issue, which is available at wileyonlinelibrary.com.]

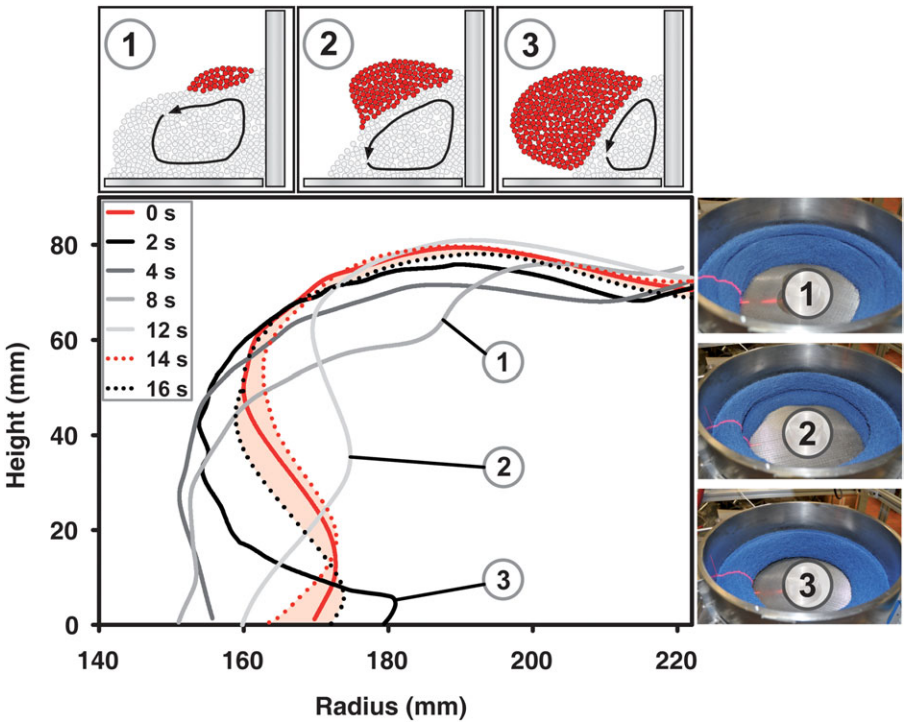

Figure 8. Position of the toroid surface with respect to time for batch M.

The red profile corresponds to the profile (0 s) taken at the beginning of one cycle. The dotted lines indicate the profiles measured just before and after the cycle was completed. The enclosed pink area between these two dotted lines indicates that the period of the cycle is around 15 s. One can also noticed the laser beam at the surface of the bed in the three snapshots corresponding to 2 s, 8 s, and 12 s. [Color figure can be viewed in the online issue, which is available at wileyonlinelibrary.com.]

measured surface profile) and the corresponding surface profile variances with respect to temperature, for the three different batches.

It can be noticed that the variance remained constant when the temperature was increased from laboratory conditions (25°C) until it reached a point where it drastically increased. This threshold temperature corresponds to the appearance of agglomerates at the toroid surface, that is to a change of flow state from FS-I to FS-II. As the coating thickness was reduced, the temperature at which the variance began to increase moved toward a higher value, as explained in section Toroid flow state FS-III. The dynamic density decreased slowly in a linear fashion with the temperature as long as agglomerates were absent. When the cohesion forces became strong enough to cause the agglomeration of particles, the linear decrease of the dynamic density was accentuated due to a larger expansion of the toroid resulting from the large particle clusters. This is evidenced by the breaking points in the dynamic density and surface variance curves, which occur at similar temperatures.

Flow state map and potential use in granulation

The applicability of the polymer coating approach to study cohesive flow in granulators is discussed in this section. Beforehand, the interparticle forces observed with a change of temperature or coating thickness are compared to other typical forces encountered during granulation using dimensional analysis.

Figure 10 displays a flow state map as a function of the dimensionless Bond number (Bo) and the modified Deborah number (De*). The latter number is obtained by dividing the value of De defined in Eq. 5 by its value at maximum shear rate (the shear rate was varied between 0.1 and 100 s^{-1}). Such normalization facilitates the comparison of different temperature/coating cases. It can be noticed from Eq. 1 to Eq. 4 that Bo and De depend, in particular, on the reptation time τ_D, the interparticle adhesion force F_{adh}, and the normal collisional velocity v_n. The interparticle cohesion force is related to the adhesive energy, which depends on the contact time t_c. The reptation time is unknown for the PEA/PMMA

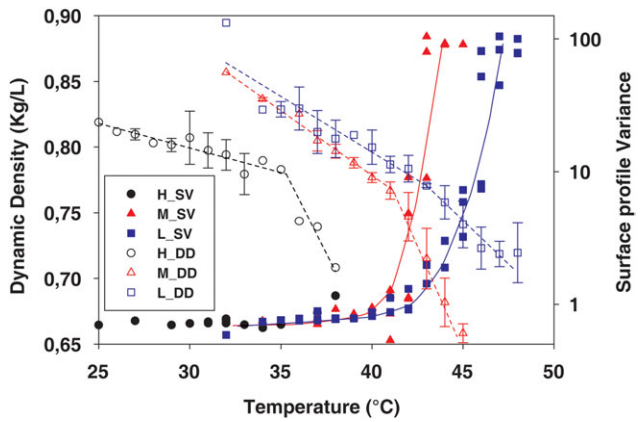

Figure 9. Dynamic density (DD) and surface profile variance (SV) with respect to the temperature for the three different batches.

[Color figure can be viewed in the online issue, which is available at wileyonlinelibrary.com.]

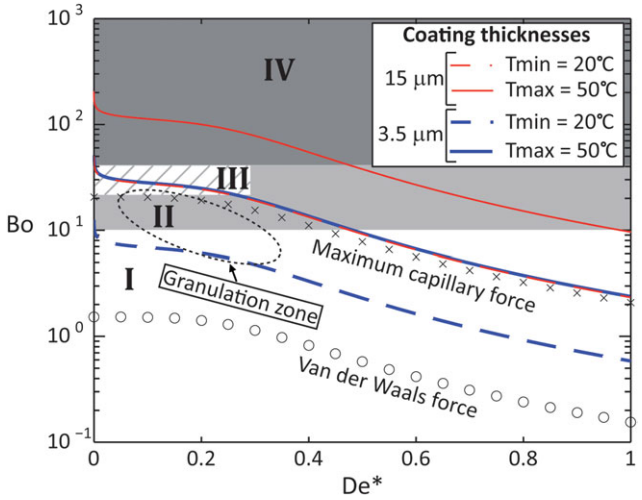

Figure 10. Flow state map associated with the cohesion induced by polymer coating in comparison with typical interparticle forces encountered in granulation.

The converted maximum capillary (surface tension = 0.073 N/m) and Van der Waals ($A_H = 6.5 \times 10^{-20}$ J and $h = 4$ Å) forces have been added for a mean particle size of 1.2 mm. The details concerning the calculation of these forces are presented in Ref. 14. The regions marked by roman numbers expose qualitatively the boundary limits of the FS. The zone inside the ellipse represents the expected flow conditions during wet granulation. [Color figure can be viewed in the online issue, which is available at wileyonlinelibrary.com.]

copolymer and its value was estimated as that of a PEA homopolymer of the same molecular weight, $\tau_R = 11.5$ s at $T_R = 291$ K, as proposed in Ref. 14. Because the T_g value for the PEA homopolymer ($\sim -20^{\circ}$C) is smaller than that for the PEA/PMMA copolymer ($\sim -6^{\circ}$C), this estimated value of the reptation time is smaller than the actual one. Using this value as a reference reptation time at 291 K, the reptation time was then calculated by means of the WLF empirical model in Eq. (1) and values $c_1 = 7,0$, $c_2 = 90$ taken from Ref. 28. The contact time was calculated while taking into account the change with temperature of the elastic modulus of the PEA/PMMA copolymer.[25] Different values of the shear rate from 0.01 to 200 s^{-1} were used to calculate the mean normal collision velocity, which are representative of the values considered in Refs. 23 and 29. Finally, it was shown in Ref. 14 that the adhesive energy increases linearly from 0.022 J/m^2 at 20°C to 0.09 J/m^2 at 50°C for a PEA/PMMA coating thickness of 120 nm. Therefore, these adhesive energies were scaled proportionally to the thickness of the polymer layer on the particles.[30]

For the spheronizer, the highest shear rate within the toroid is found near the rotating disc (highest De* value) and the lowest near the surface in the vicinity of the wall (lowest De* value).[23] Each curve presented in Figure 10 was obtained by varying the shear rate and can then be seen as the profile of cohesion in the particle bed from the surface of the toroid toward the a position near of the spheronizer disc as De* increases. Flow state regions have been added to the graph on the basis of the results presented earlier for varying temperatures and coating thicknesses. Note that the concept of flow state is a local one as it may and often does change from the surface of the toroid to the vicinity of the spheronizer disc. For example, the top-most curve, corresponding to a 15-μm coating thickness and a temperature of 50°C, shows that, under these conditions, the surface of the toroid is in flow state FS-IV, its core region in flow state FS-II, and its bottom, near the disc, in free-flowing agglomerate-free flow state FS-I. It is true; however, that these FS were defined from observations at the surface of the bed. FS-I was observed to extend to Bo values around 10 with the absence of agglomerates in this range, which complies with the findings of McCarthy et al.[31] as regards weakly cohesive particle flow. Values of Bo between 10 and 40 led to strongly cohesive flow behavior and are represented by FS-II, which is in agreement with the work of Khinast et al.[5] FS-III is a difficult state to position within the graph because it is characterized by two particle layers that present different shear rate intensities along with a periodic behavior. Another difficulty comes from the fact that this state was not observed in the case of batch **L** and it did not exist for a long enough period of time for batch **H**. FS-III requires that the shear rate and the adhesion force at the surface in the vicinity of the spheronizer wall are sufficiently low to sustain a secondary layer. The FS-III zone in Figure 10 was set accordingly and shows that the two curves corresponding to 15 μm (20°C) and 3.5 μm (50°C) represent cases where FS-III was observed. Finally, FS-IV was placed in the graph for Bond numbers higher than 40, which corresponds to the experimental observations for batches **M** and **H**.

To compare the Bond number of the polymer coating layers to the forces encountered in granulation systems, two common interparticle forces found in such processes, let alone the capillary and van der Waals forces, have been added to Figure 10. As a general indication, a dashed ellipse representing the common operation zone of granulators and covering three FS has also been added to the graph. As can be seen, the capillary force curve lies between Bond numbers 2 and 20. As expected, the van der Waals forces do not have a significant impact for the mean particle size considered (1.2 mm) in this work, as the related curve lies in a region where Bo < 1.

The use of the polymer coating approach allowed modifying significantly the flow behavior in the spheronizer as described by the different flowing states and the dynamic density values representing the bulk cohesivity of the particle bed. Because the method can be used without affecting the PSD, its employment in a spheronizer that mimics particle flow in granulation equipment sheds light on the impact of cohesion on the progression of more complex granulation processes.

In Figure 10, the wet granulation zone indicates that the flow state FS-II should be observed under efficient operating conditions. In FS-II, the particles are mixed homogeneously during the operation and the interparticle forces are strong enough to promote their agglomeration. These two operational characteristics are not found for the other FS. The interparticle forces are too weak in FS-I and do not promote the particle agglomeration. Moreover, the flow pattern is divided into two different zones in FS-III and the particles do not mix at all in FS-IV.

The granulation zone is bounded above by a Bond number close to the maximum capillary force curve where the particle bed becomes binder saturated. If this limit is surpassed, it means that the maximum capillary force is reached, which can potentially cause the flow state to migrate from FS-II to

FS-III and lead to a fast and difficult to control particle growth. The granulation zone is bounded below by a Bond number associated with small interparticle forces that are too weak to promote particle agglomeration found in FS-II. In a granulation process, such a phenomenon is observed when the binder content is too low. The granulation zone is also limited by Deborah number values which can be directly linked to the intensity of shear rate provided by an agitator or a rotating disc, for example. The minimum Deborah number corresponds to a low shear rate (slow agitator or disc speed) and relatively poor particle mixing, which is typical of the FS-III behavior. The maximum Deborah number corresponds to high shear rate (high agitator or disc speed), which favors particle breakage and prevents particle agglomeration. Note that the granulation zone presented here is a general indication of where the process should be operated to obtain a homogeneous product with optimal performance. The binder content that affects the interparticle forces, and the speed of the agitator should be set to obtain the FS-II behavior. On the other hand, their exact values should be determined according to the desired product properties, which also depend on the evolution of the particle flow during the whole operation.

Recently, the flow behavior in a high shear granulation process was evaluated in 3-D with a nonintrusive positron emission particle tracking (PEPT) method.[9] The results revealed the existence of different regions with characteristic flow patterns that change over time. To accumulate enough data to represent these flow patterns, a 35-minutes granulation run was divided into seven smaller time periods. It resulted in a characterization of the particle flow during a period of 5 min and led to a rough estimation of the velocity profile and the residence time of the PEPT tracer within the particle bed. A longer data acquisition time could be considered to refine the information obtained so far, but this assumes that the flow patterns remain stable during the measurement. The use of polymer coating offers the possibility to control the interparticle forces without affecting the PSD. It means that specific flow patterns representative of those in a granulation system at a specific time could be reproduced and characterized easily with this method.

Conclusions

This work used inert particles coated with a layer of a PEA/PMMA copolymer to investigate how temperature-dependent interparticle forces affect the flow behavior in a spheronizer. Four different FS were observed depending on the temperature of the particle bed. The FS-I is associated with free-flowing behavior of the particles and was observed near the ambient laboratory conditions. The FS-II is characterized by agglomerates appearing at the surface of the particle bed, the size of which increases as the temperature is incremented. The third flow state concerns the formation of a secondary layer of agglomerated particles whose volume changes in a periodic fashion with time. The FS-IV is characterized by a solid-like motion as the particles are completely agglomerated. A flow map presenting the flowing states was derived to show the potential use of the polymer coating approach for mimicking the flow behavior in granulation processes. A more elaborate characterization of the forces between PEA/PMMA copolymer layers will be done in a near future so as to gain more insight into the interdiffusion rate and the increase of adhesive energy with respect to temperature and contact time. These measurements will help refine the model parameters used in this work and, thus, improve the predictability of the phenomena observed. These measurements will also help develop a cohesive force model for the discrete element simulation of the particle flow dynamics in the spheronizer considered in this work or other related granulation processes.

Acknowledgments

The financial support of the Natural Sciences and Engineering Research Council of Canada (NSERC), Merck Frosst of Canada, and Ratiopharm is gratefully acknowledged. The authors thank the support of Mr. David Dube for the development of the acquisition program used with the laser profiler.

Literature Cited

1. Lekhal A, Conway SL, Glasser BJ, Khinast JG. Characterization of granular flow of wet solids in a bladed mixer. *AIChE J*. 2006;52(8):2757–2766.
2. Li HM, McCarthy JJ. Cohesive particle mixing and segregation under shear. *Powder Technol*. 2006;164(1):58–64.
3. Faqih A, Chaudhuri B, Muzzio FJ, Tomassone MS, Alexander A, Hammond S. Flow-induced dilation of cohesive granular materials. *AIChE J*. 2006;52(12):4124–4132.
4. Chaudhuri B, Mehrotra A, Muzzio FJ, Tomassone MS. Cohesive effects in powder mixing in a tumbling blender. *Powder Technol*. 2006;165(2):105–114.
5. Khinast JG, Radl S, Kalvoda E, Glasser BJ. Mixing characteristics of wet granular matter in a bladed mixer. *Powder Technol*. 2010;200(3):171–189.
6. Iveson SM. Limitations of one-dimensional population balance models of wet granulation processes. *Powder Technol*. 2002;124(3):219–229.
7. Fan XF, Yang ZF, Parker DJ, Ng B, Ding YL, Ghadiri M. Impact of surface tension and viscosity on solids motion in a conical high shear mixer granulator. *AIChE J*. 2009;55(12):3088–3098.
8. Forrest S, Bridgwater J, Mort PR, Litster J, Parker DJ. Flow patterns in granulating systems. *Powder Technol*. 2003;130(1–3):91–96.
9. Saito Y, Fan XF, Ingram A, Seville JPK. A new approach to high-shear mixer granulation using positron emission particle tracking. *Chem Eng Sci*. 2011;66(4):563–569.
10. Wang FY, Cameron IT. Review and future directions in the modelling and control of continuous drum granulation. *Powder Technol*. 2002;124(3):238–253.
11. Perry RH, Green DW. *Perry's Chemical Engineers' Handbook, 2008*. McGraw-Hill: New York. Available at: http://site.ebrary.com/id/10211725. Accessed on October 3, 2011.
12. Litster JD, Hapgood KP, Michaels JN, Sims A, Roberts M, Kameneni SK. Scale-up of mixer granulators for effective liquid distribution. *Powder Technol*. 2002;124(3):272–280.
13. Rudolph V, Rasul MG, Carsky M. Segregation potential in binary gas fluidized beds. *Powder Technol*. 1999;103(2):175–181.
14. Bouffard J, Bertrand F, Chaouki J, Giasson S. Control of particle cohesion with a polymer coating temperature adjustments. *AIChE J*. 2012;58(12):3685–3696.
15. Schach R, Creton C. Adhesion at interfaces between highly entangled polymer melts. *J Rheol*. 2008;52(3):749–767.
16. Timoshenko S, Goodier JN. *Théorie de l'élasticité*. Paris: C.Béranger, 1961.
17. Zhang DZ, Rauenzahn RM. Stress relaxation in dense and slow granular flows. *J Rheol*. 2000;44(5):1019–1041.
18. Chau KW, Swei GS. Contact time and interfacial fracture energy of tacky polymers. *J Polym Sci Pol Phys*. 2004;42(16):3013–3025.
19. Barthel E. Adhesive elastic contacts: JKR and more. *J Phys D Appl Phys*. 2008;41(16):1–20.
20. Brilliantov NV, Albers N, Spahn F, Poschel T. Collision dynamics of granular particles with adhesion. *Phys Rev E*. 2007;76(5):1–12.
21. Liechti KM, Xu DW, Ravi-Chandar K. On the modified Tabor parameter for the JKR-DMT transition in the presence of a liquid meniscus. *J Colloid Interf Sci*. 2007;315(2):772–785.
22. Pingali KC, Shinbrot T, Hammond SV, Muzzio FJ. An observed correlation between flow and electrical properties of pharmaceutical blends. *Powder Technol*. 2009;192(2):157–165.

23. Bouffard J, Bertrand F, Chaouki J, Dumont H. Discrete Element Investigation of Flow Patterns and Segregation in a Spheronizer. doi:10.1016/j.compchemeng.2012.09.023.
24. Sinha SK, Briscoe BJ. *Polymer Tribology*. London: Imperial College Press, 2009.
25. Lafferty SV, Newton JM, Podczeck F. Kinetic examination of the mechanical transition of polymethyl methacrylate films prepared from aqueous dispersions. *Int J Pharm*. 2002;239(1–2):179–183.
26. Abdullah EC, Geldart D. The use of bulk density measurements as flowability indicators. *Powder Technol*. 1999;102(2):151–165.
27. Zhu HP, Zhou ZY, Yang RY, Yu AB. Discrete particle simulation of particulate systems: Theoretical developments. *Chem Eng Sci*. 2007;62(13):3378–3396.
28. Andreozzi L, Castelvetro V, Faetti M, Giordano M, Zulli F. Rheological and thermal properties of narrow distribution poly(ethyl acrylate)s. *Macromolecules*. 2006;39(5):1880–1889.
29. Corwin EI. Granular flow in a rapidly rotated system with fixed walls. *Phys Rev E*. 2008;77(3):1–8.
30. Luengo G, Pan J, Heuberger M, Israelachvili JN. Temperature and time effects on the "adhesion dynamics" of poly(butyl methacrylate) (PBMA) surfaces. *Langmuir*. 1998;14(14):3873–3881.
31. McCarthy JJ, Nase ST, Vargas WL, Abatan AA. Discrete characterization tools for cohesive granular material. *Powder Technol*. 2001;116(2–3):214–223.

Manuscript received Nov. 17, 2011, revision received Aug. 7, 2012, and final revision received Oct. 22, 2012.